OPEN ACCESS Freely available online

ISSN 2737-5323
Volume 5, Issue 2
https://afm.iikii.com.sg
Applied Functional Materials

Article

Powder X-ray Line Diffraction Study on Mono Sodium L-glutamate Pentahydrate by Whole Powder Pattern Fitting Analysis

Md. Khalid Hossain Shishir [1], Allah Rakha Aidid [1], Sahil Aman [1], and Md. Ashraful Alam [2,*]

[1] partment of Applied Chemistry and Chemical Engineering, Islamic University, Kushtia-7003, Bangladesh; e-mail@e-mail.com
[2] Institute of Glass and Ceramic Research and Testing (IGCRT), Bangladesh Council of Scientific and Industrial Research (BCSIR), Dhaka-1205, Bangladesh
* Correspondence: ashrafulalam@bcsir.gov.bd

Received: May 28, 2025; **Revised:** Jun 07, 2025; **Accepted:** Jun 08, 2025; **Published:** Jun 30, 2025

Abstract: The crystallographic bibliography of mono Sodium L-glutamate Pentahydrate (MSLGPH) found unique unparalleled structural geometry using powder X-ray diffraction (XRD). The XRD analysis revealed the atomic structure of MSLGPH crystals providing a detailed refinement of lattice parameters and crystal symmetry of orientation. Crystallography revealed dislocation density of 2.009 × 10^{-4} nm^{-2}, crystallinity index of 1.98, unit cell density of 1.48 g/cm^3 and specific surface area of 57.46 m^2/g, contributing to unique structural geometry. Rietveld refinement confirmed a unified 100 % crystalline phase using the WPPF method. The calculated lattice parameters are a= 6.224, b= 16.669, c= 5.992 Å; α= 98.77, β= 99.83, γ= 98.54° in a triclinic crystal system with lattice volume of 595.565 $Å^3$ and strain of 0.163 %. The strongest diffraction distinct 2θ at 20.364° (0-31) plane. Various models were used to estimate crystallite size, with the Scherrer equation exploring an average crystallite size of 70.55 nm for nano confirmation.

Keywords: MSLGPH, Structural geometry, Triclinic, WPPF, XRD

1. Introduction

MSLGPH is a hydrated form of crystalline monosodium glutamate (MSG), a common flavor enhancer [1]. Its chemical formula is $C_5H_8NNaO_4$. $5H_2O$, indicating that each MSG molecule is associated with five water molecules in its crystal symmetry [2]. The crystalline MSLGPH is significant in food science [2]. The pentahydrate form influences its stability, solubility and crystallinity in functional applications [3]. The crystallography of MSLGPH is important because it reveals crucial compound structure and properties [4]. Without understanding its crystal structure, cannot optimize its use in food industries, ensures quality control in production [5]. This phenomenon is vital for improving manufacturing processes, enhancing product stability and potentially discovering new applications in food nanoscience and pharmaceuticals [6]. Point this drawback, studying its hydrated interact within crystal structures of MSLGPH exploring crystalline behavior is the prime focus of this study.

2. Materials and Methods

Materials and Methods should be described with sufficient details to allow others to replicate and build on published results. Please note that publication of your manuscript implicates that you must make all materials, data, computer code, and protocols associated with the publication available to readers. Please disclose at the submission stage any restrictions on the availability of materials or information. New methods and protocols should be described in detail while well-established methods can be briefly described and appropriately cited.

Research manuscripts reporting large datasets that are deposited in a publicly available database should specify where the data have been deposited and provide the relevant accession numbers. If the accession numbers have not yet been obtained at the time of submission, please state that they will be provided during review. They must be provided before publication.

Interventional studies involving animals or humans, and other studies require ethical approval must list the authority that provided approval and the corresponding ethical approval code.

3. Characterization

The geometrical characteristics of crystal symmetry and lattice parameters were analyzed by multipurpose XRD instrument SmartLab SE [Rigaku, Japan]. The typical X-rays produced by the copper X-ray tube [CuKα, λ= 1.54060 Å] had a voltage of 40.0 kV and a current of 50.0 mA [7, 8]. Data were obtained from 5 ° to 100 ° with 0.01° step intervals. To explore the desired CuKα beam, a Ni-Kβ filter was added to the diffracted beam path to minimize Kβ-rays. All experiments employed Bragg-Brentano (BB) para-focusing geometry. The analysis was performed in standard mode, with a 1D scan at a 10 °/min rate and HPAD featured the Hypix-400 horizontal detector [9, 10]. Horizontal theta-theta goniometer was employed and both slit boxes 1.0 and 2.0 were open. Data was characterized using SmartLab Studio II software with ICDD PDF-5+ standard data [11]. The distance between atomic planes in a crystal system is represented by d-spacing (d) values computed by Bragg's law [12, 13]. The average crystallite sizes were determined using various models. Multiple studies have utilized different models for calculating crystallite size, and the related equations are listed below [14, 15].

Bragg's law: $$d = \frac{n\lambda}{2\sin\theta} \quad (1)$$

Scherrer equation: $$D_s = \frac{K\lambda}{\beta \cos\theta} \quad (2)$$

Williamson-Hall method: $$\beta_{total} \cos\theta = \frac{k\lambda}{D} + 4.\varepsilon \sin\theta \quad (3)$$

Monshi-Scherrer method: $$ln(\beta) = ln\frac{1}{cos\,\theta} + ln\frac{k\lambda}{D} \quad (4)$$

Linear straight-line model: $$\cos\theta = \frac{k\lambda}{D} \times \frac{1}{\beta} \quad (5)$$

Sahadat-Scherrer model: $$\cos\theta = \frac{k\lambda}{D_{s-s}} \times \frac{1}{FWHM} \quad (6)$$

Size-strain plot model: $$(d_{hkl}\,\beta_{hkl}\cos\theta)^2 = \frac{k\lambda}{D}(d_{hkl}{}^2\beta_{hkl}\cos\theta) + \frac{\varepsilon^2}{4} \quad (7)$$

Halder-Wagner method: $$\left(\frac{\beta_{hkl}}{d_{hkl}}\right)^2 = \left(\frac{1}{D}\right)\left(\frac{\beta_{hkl}}{d_{hkl}^2}\right) + \left(\frac{\varepsilon}{2}\right)^2 \quad (8)$$

The quantitative analysis was performed using the whole powder pattern fitting (WPPF) method and structural symmetry was explored using VESTA software.

4. Result and Discussion

4.1 Crystallographic Phase Analysis

The XRD pattern of the MSLGPH nanoparticles was obtained. All the diffractions were identified as belonging to the Triclinic (anorthic) phase of MSLGPH, in accordance with ICDD data [Card No. 02-069-1324], as shown in Fig. 1(a). The observed diffraction broadening in the XRD pattern strongly indicates the presence of small nanocrystals in the samples, with no evidence of impurities. The analysis identified nine main diffractions at 2θ angles of 15.541, 20.364, 23.549, 25.609, 26.759, 28.045, 31.026, 35.894 and 46.592°, with corresponding crystallite sizes of 58.00, 88.50, 85.00, 63.90, 46.90, 61.20, 55.10, 65.90 and 110.40 nm, as shown in Table 1. These diffraction patterns are mainly associated with the MSLGPH phase, identified at the (101), (0-31), (1-21), (111), (050), (140), (-102), (1-61) and (003) planes, according to ICDD standard [Card No. 02-069-1324]. The corresponding d-spacing values of 0.56973, 0.43573, 0.37748, 0.34756, 0.33289, 0.31790, 0.28801, 0.24998, and 0.19477 nm closely match the standard ICDD data. The recorded intensities for these planes were 7779 (30.55 %), 25461 (100.0 %), 9721 (38.18 %), 18497 (72.65 %), 2936 (11.53 %), 5700 (22.39 %), 6531 (25.65 %), 2149 (8.44 %) and 2758 (10.83 %) counts per second (cps), with peak heights of 43092, 176530, 68926, 105698, 13671, 32237, 28197, 11061 and 20888 cps, as shown in Table 1. The increased intensity (I.) observed in the MSLGPH nanocrystals suggests a high crystallinity (47.50 %). The primary diffraction for the nanocrystal at 20.199 (0-31) in the ICDD data shifted right to 20.364 (0-31) in the experimental data, as shown in Fig. 1(b).

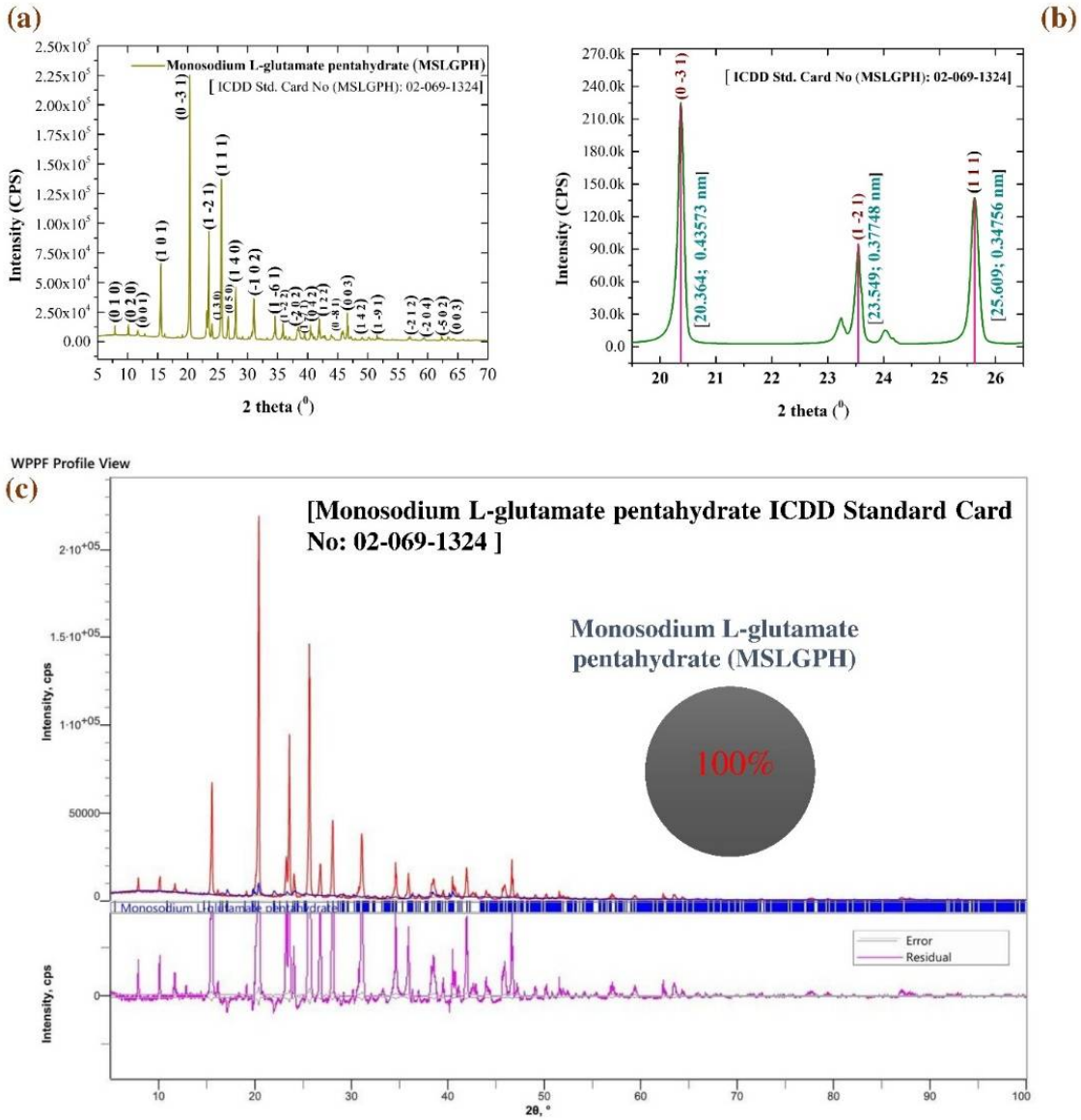

Fig. 1 (**a**) X-ray diffraction pattern, (**b**) peak illustration and (**c**) quantitative analysis in whole powder fitting method of investigated MSLGPH.

A rightward shift in the 2θ value for MSLGPH crystal indicates a reduction in the lattice spacing (d-spacing) according to Bragg's law. This shift suggests structural changes within the crystal, such as strain, compression, or alterations in interatomic distances. In crystallography, this shift may also point to variations in the sample's composition, defects, or interactions with external factors like temperature or pressure [7]. Fig. 1(c) depicted 100.0 % MSLGPH nanocrystals under different fitting conditions [Rwp: 59.51 %, Rp: 47.82 %, S: 8.8316, χ^2: 77.9964]. The calculated lattice parameters of the MSLGPH nanocrystals are a= 6.224, b= 16.669 and c= 5.992 Å; α= 98.77, β= 99.83 and γ= 98.54°, with a lattice volume of 595.565 Å^3 and a lattice strain of 0.163 %. The crystallographic analysis revealed dislocation density of 2.009 × 10^{-4} nm^{-2}, crystallinity index of 1.98, unit cell density of 1.48 g/cm^3 and specific surface area of 57.46 m^2/g which explored and conformation of high crystallographic MSLGPH were observed [10, 11].

Table 1. Grain size calculation and crystallographic bibliography of MSLGPH.

Grain size calculation of MSLGPH						
Diffraction angle (2Θ)	**Theta(Θ)**	**d-spacing d (±0.001) nm**	**Height (cps)**	**FWHM (radians)**	**Crystallite size D (±0.01) nm**	**Reflection**
15.541	7.770	0.56973	43,092	0.144	58.00	(101)
20.364	10.182	0.43573	1,76,530	0.095	88.50	(0-31)

23.549	11.774	0.37748	68,926	0.100	85.00	(1-21)
25.609	12.804	0.34756	1,05,698	0.133	63.90	(111)
26.759	13.379	0.33289	13,671	0.182	46.90	(050)
28.045	14.022	0.31790	32,237	0.140	61.20	(140)
31.026	15.513	0.28801	28,197	0.156	55.10	(-102)
35.894	17.947	0.24998	11,061	0.132	65.90	(1-61)
46.592	23.296	0.19477	20,888	0.082	110.40	(003)

Simple peak indexing of MSLGPH

2Θ	**Θ**	**1000× $Sin^2Θ$**	**Reflection**	**Remarks**
20.364	10.182	31.249	(0-31)	$0^2+(-3)^2+1^2=10$
23.549	11.774	41.637	(1-21)	$1^2+(-2)^2+1^2=6$
25.609	12.804	49.113	(111)	$1^2+1^2+1^2=3$

Peak indexing from d-spacing of MSLGPH

2Θ	**Θ**	**d (Å)**	**$1000/d^2$**	**Reflection**	**Remarks**
20.364	10.182	4.3573	52.670	(0-31)	$0^2+(-3)^2+1^2=10$
23.549	11.774	3.7748	70.179	(1-21)	$1^2+(-2)^2+1^2=6$
25.609	12.804	3.4756	82.782	(111)	$1^2+1^2+1^2=3$

Comparison of Experimental (Exp.) and Standard (Std.) Diffraction Data

2Θ		**Inter planer distance (d) (Å)**		**Norm. I. (%)**	
(Exp.)	(Std.)	(Exp.)	(Std.)	(Exp.)	(Std.)
20.364	20.199	4.3573	4.3925	100.0	100.0
23.549	23.594	3.7748	3.7676	38.18	42.84
25.609	25.299	3.4756	3.5175	72.65	25.32

Quantitative analysis of MSLGPH by WPPF

Pattern fitting condition	**Phase (%)**	**Crystallinity & Strain (%)**	**Lattice volume, ($Å^3$)**	**Lattice parameters**
Rwp, % 59.51; Rp, % 47.82; S, 8.8316; χ^2, 77.9964.	100.0	47.50; 0.163	595.565	a= 6.224, b= 16.669, c= 5.992 Å; α= 98.77, β= 99.83, γ= 98.54°
ICDD (PDF-5+) [Card No: 02-069-1324]		a:6.116Å b:16.511Å c: 6.007Å α:97.51° β:100.94° γ:98.20°; [Xtl Cell Z:1.00 c/a:0.982 a/b:0.370 c/b:0.364]; Space Group: P1(1); MolecularWt:518.38 g/mol.		

4.2 Estimation of Crystallite Size Using Models

The average crystallite size of the MSLGPH crystal was found to be 70.55 nm using the Scherrer equation, while the Williamson-Hall plot gave a value of 89.47 nm. The Monshi-Scherrer method produced 78.32 nm, the Linear straight-line model resulted in 3785.76 nm, the Sahadat-Scherrer model gave 92.46 nm, the Size-strain plot model yielded 85.61 nm, and the Halder-Wagner method calculated 237.52 nm that shown in Fig. 2. The calculated microstrain from the Williamson-Hall plot model was 4.86472×10^{-4}.

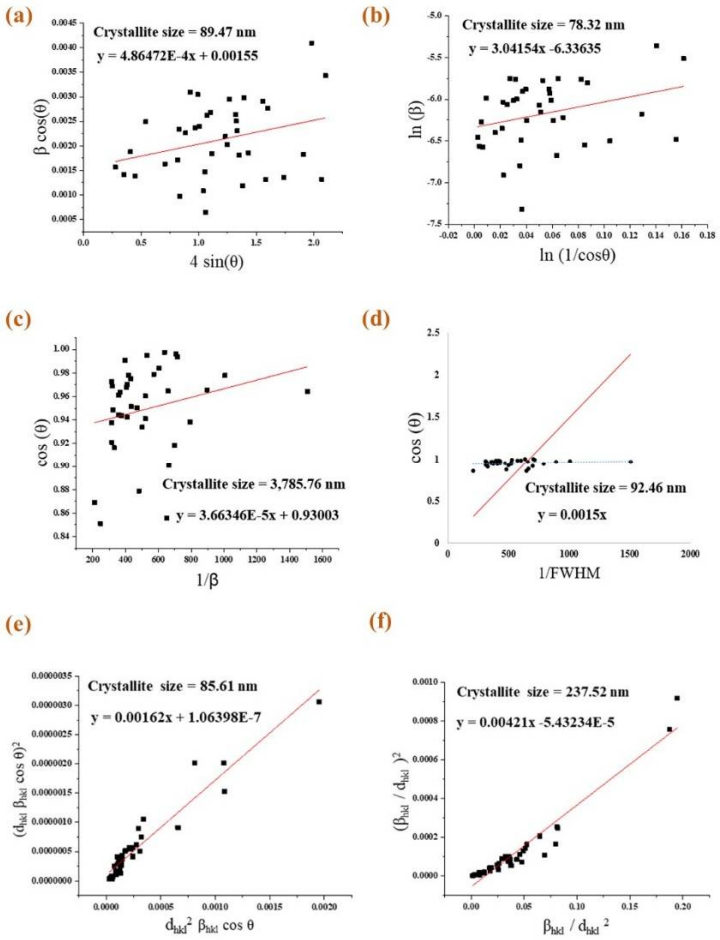

Fig. 2. Estimation of crystallite size using (**a**) Williamson-Hall plot, (**b**) Monshi-Scherrer method, (**c**) Linear straight-line model, (**d**) Sahadat-Scherrer model, (**e**) Size-strain plot model, (**f**) Halder-Wagner method for MSLGPH crystal.

4.3 Structural Mechanism Analysis

The structures shown in Fig. 3 were created using VESTA [visualization for electronic and structural analysis] software. The Triclinic structure was based on space group P1 (1) with unit cell edge lengths of a= 6.224 Å, b= 16.669 Å, and c= 5.992 Å, and angular parameters α= 98.77°, β= 99.83°, and γ= 98.54°. The crystal shape of the Triclinic was identical and lattice parameters like axial and angular parameters depicted the atom distribution and volume.

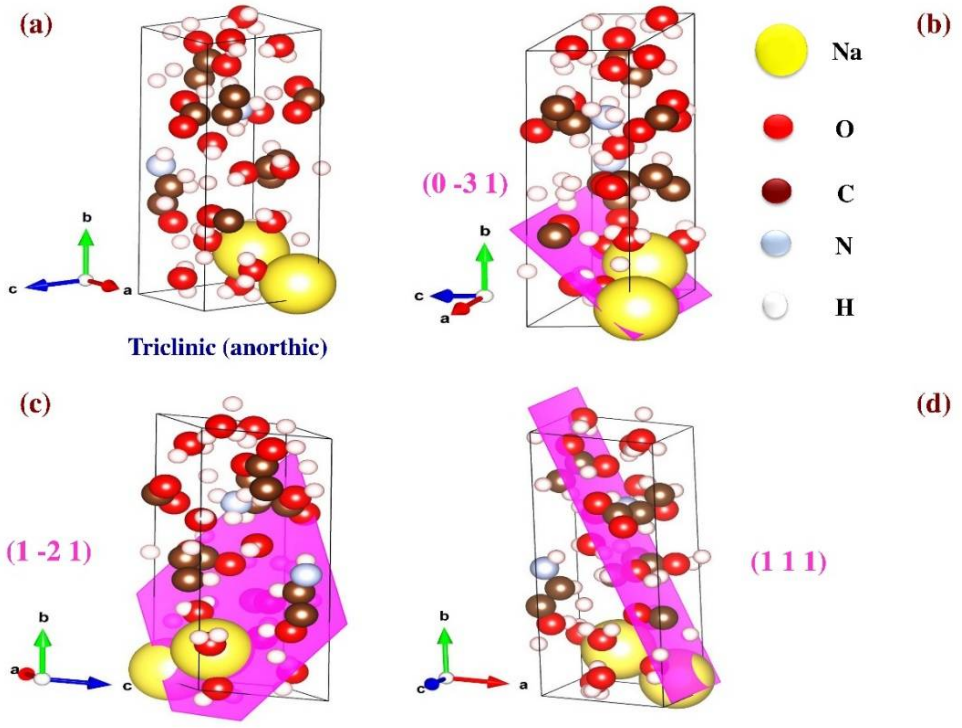

Fig. 3. (**a**) Structural symmetry of triclinic, (**b**) (0-31), (**c**) (1-21) and (**d**) (111) plane of MSLGPH.

The structural analysis of the edge and corner shows the atoms were uniformly oriented in the uniform direction. Fig. 3 illustrates the crystal structure and predominant planes of the MSLGPH crystal where 3(a) depicts the ball-and-stick model, 3(b) (0-31), 3(c) (1-21) and 3(d) (111) plane in 3D space shows for crystal growth and orientation geometry of uniformly distributed atom onto the crystal plane. The plane (0-31), (1-21) and (111) were oriented in identical direction also observed on the predominant zone axis.

5. Conclusions

The XRD analysis of MSLGPH revealed its crystallographic properties in detail. The study confirmed a fully crystalline triclinic structure with precise lattice parameters and crystal symmetry. Various crystallite size estimation methods were employed, with the Scherrer equation indicating an average size of 70.55 nm. We also determined other important crystallographic characteristics such as dislocation density, crystallinity index, unit cell density and specific surface area of the nanocrystals. These findings contribute significantly to understanding the structural properties of MSLGPH and may aid in controlling its crystal growth for functional applications.

Funding: This research did not receive external funding.
Data Availability Statement: Not applicable.
Acknowledgments: The author heartiest thanks to Dr. Shirin Akter Jahan, Principal Scientific Officer (PSO), BCSIR, Bangladesh for using the software, PC and other appliances.
Conflicts of Interest: The authors declare no conflict of interest.

Reference

1. Longden, J.P. A Method for the Quantitative Recovery of Mononucleotides from Fermentation Waste by Precipitation. Master's Thesis, Lancaster University, UK. 2015. https://www.proquest.com/openview/35695461088e8f55a04e48395bae67a8/1?pqorigsite=gscholar&cbl=2026366&diss=y
2. Kashiwagi, T.; Sano, C.; Kawakita, T.; Nagashima, N. Monosodium l-Glutamate Pentahydrate. *Cryst. Struct. Commun*. **1995**, *51* (6), 1053–1056. https://doi.org/10.1107/S0108270194014472
3. Perea, C.G.; Ihle, C.F.; Dyer, L.; et al. Copper Sulfide Precipitation from Alkaline Monosodium Glutamate Solutions. *Miner. Eng*. **2024**, *215*, 108816. https://doi.org/10.1016/j.mineng.2024.108816

4. Ahmed, S.; Shishir, M.K.H.; Sadia, S.I.; et al. Crystallographic Phase Biographs of Copper Nanocrystalline Material: A Statistical Perspective Review. *Nano-Struct. Nano-Objects* **2024**, *39*, 101275. https://doi.org/10.1016/j.nanoso.2024.101275
5. Al-Mahmud, M.R.; Shishir, M.K.H.; Ahmed, S.; et al. Stoichiometry Crystallographic Phase Analysis and Crystallinity Integration of Silver Nanoparticles: A Rietveld Refinement Study. *J. Cryst. Growth* **2024**, *643*, 127815. https://doi.org/10.1016/j.jcrysgro.2024.127815
6. Hossain, M.S.; Ahmed, S. Sustainable Synthesis of Nano CuO from Electronic Waste (E-waste) Cable: Evaluation of Crystallite Size via Scherrer Equation, Williamson-Hall Plot, Halder-Wagner model, Monshi-Scherrer Model, Size-Strain Plot. *Results Eng.* **2023**, *20*, 101630. https://doi.org/10.1016/j.rineng.2023.101630
7. Pandey, A.; Dalal, S.; Dutta, S.; et al. Structural Characterization of Polycrystalline Thin Films by X-ray Diffraction Techniques. *J. Mater. Sci. - Mater. Electron.* **2021**, *32*, 1341–1368.
8. Alam, M.A.; Shishir, M.K.H.; Sarkar, D.; et al. X-ray Line Diffraction Study of Preferred Oriented Hexagonal Zincite Nanocrystals: A Crystallographic Investigation. *J. Cryst. Growth* **2025**, 128230. https://doi.org/10.1016/j.jcrysgro.2025.128230
9. Aidid, A.R.; Shishir, M.K.H.; Rahaman, M.A.; et al. Powder X-ray Line Diffraction Pattern Profiling of Anatase-Quartz Binary Oxide: A Crystallographic Investigation. *Next Mater.* **2025**, *8*, 100571. https://doi.org/10.1016/j.nxmate.2025.100571
10. Islam, M.; Islam, M.T.; Shishir, M.K.H.; et al. X-ray Crystallographic Structural Profiling of Polyvinyl Alcohol (PVA) Capped Nickel Oxide Nanoparticle. *Nano Trends* **2025**, *10*, 100106. https://doi.org/10.1016/j.nwnano.2025.100106
11. Ahmed, S.; Shishir, M.K.H.; Islam, M.T.; et al. Crystallinity Integration of Anatase (TiO2) Nanocrystal by Whole Powder Pattern Fitting (WPPF) Method: A Rietveld Refinement Study. *Results Mater.* **2025**, *26*, 100673. https://doi.org/10.1016/j.rinma.2025.100673
12. Alam, M.A.; Ahmed, S.; Bishwas, R.K.; et al. Crystal Growth Behavior Interpret of Co-precipitated Derived Nickel Oxide (NiO) Nanocrystals. Nano-Struct. *Nano-Objects* **2025**, *42*, 101494. https://doi.org/10.1016/j.nanoso.2025.101494
13. Ahmed, S.; Alam, M.A.; Sadia, S.I.; et al. Stoichiometry Low-temperature Dynamics Crystal Growth Interpret of Zinc Oxide Hexagonal Nanocrystals. *Next Mater.* **2025**, *7*, 100636. https://doi.org/10.1016/j.nxmate.2025.100636
14. Ray, G.; Haque, I.; Ahmed, T.; et al. Synthesis of Carbon Capturing NaX Zeolite from Rice Husk Ash: Evaluation of Its Adsorption Properties. *ACS Sustain. Resour. Manag.* **2025**, *2*(4), 662–672. https://doi.org/10.1021/acssusresmgt.5c00019
15. Sachchu, M.M.H.; Anik, F.K.; Ahmed, S.; et al. Crystallographic Investigation of PVA@PLA Nanocomposite Film by X-ray Diffraction: Insight from High Resolution TEM. *J. Eng. Res. Rep.* **2025**, *27* (3), 310–327. https://doi.org/10.9734/jerr/2025/v27i31436